

Initial operation of a real-time Thomson scattering evaluation system on the Large Helical Device

K.C. Hammond,^{1, a)} F.M. Laggner,¹ A. Diallo,¹ S. Daskoczynski,¹ C. Freeman,¹ H. Funaba,² D.A. Gates,¹ R. Rozenblat,¹ G. Tchilinguirian,¹ Z. Xing,³ I. Yamada,² R. Yasuhara,² and E. Kolemen,^{1, 3}

¹⁾Princeton Plasma Physics Laboratory, Princeton, NJ, USA

²⁾National Institute for Fusion Science, Toki, Japan

³⁾Princeton University, Princeton, NJ, USA

(Dated: 25 November 2023)

A scalable system for real-time analysis of electron temperature and density based on Thomson scattering signals, initially developed for and installed on the NSTX-U experiment, was recently adapted for the Large Helical Device (LHD) and operated for the first time during plasma discharges. The system consists of fast digitizers and a server with multiple parallel-operating CPUs, each of which infers temperature and density values for a spatial point in the LHD plasma. During its initial operation, it routinely recorded and processed signals for four spatial points at the laser repetition rate of 30 Hz, well within the system's rated capability for 60 Hz. We present examples of data collected from this initial run and describe subsequent adaptations to the analysis code to improve the fidelity of the temperature calculations.

I. INTRODUCTION

The ability to determine plasma temperature and density profiles in real time is valuable to plasma control systems seeking to optimize plasma properties or maintain device safety. The Thomson scattering diagnostic is an attractive candidate for real-time profile evaluation due to its ability to make non-invasive measurements of electron temperature T_e and electron density n_e throughout a typical fusion plasma.¹ In addition, the localized nature of the measurement obviates the need for intermediate analysis such as tomographic inversion or equilibrium modeling to infer the profiles.

Systems for evaluation of T_e and n_e from Thomson scattering data in real time have been developed for a number of devices over the years.²⁻⁶ In this work, we use a framework developed recently for NSTX-U.⁷ Its main components are a set of fast digitizers and a multi-core server. The digitizers collect signals from the detection electronics. The server employs real-time software to calculate T_e and n_e from the signals between subsequent laser pulses, supporting repetition rates of up to 60 Hz.⁸ The server outputs values of T_e , T_e uncertainty, n_e , and n_e uncertainty for each scattering volume as analog signals that may be fed into real-time control systems.

The setup was subsequently replicated and installed on the Large Helical Device (LHD) to evaluate signals from the LHD Thomson scattering system. This system currently employs four Nd:YAG lasers that enable pulse repetition rates ranging from 10 to 100 Hz.⁹ As depicted in Fig. 1, the laser beam line extends radially through a horizontally-elongated plasma cross-section. The collection optics observe backscattered light, which is transmitted through optical fibers to a set of 144 polychromators.^{10,11} Within each polychromator, the scattered light is passed through bandpass filters to six avalanche photodiodes (APDs).¹² Signals from five of these APDs are used for T_e and n_e evaluation during plasma discharges, and

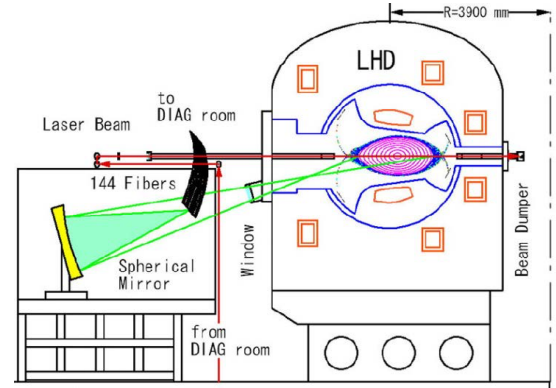


FIG. 1. Schematic of the LHD Thomson scattering system. Reproduced with permission from Ref. 12.

the remaining signal is used for Rayleigh calibration.¹³ As the polychromator setup used in LHD is similar to what is employed in NSTX-U,^{14,15} the real-time framework could be adapted for use on LHD with minor software modifications.

During its initial operation on LHD, the real-time system collected and evaluated signals from four polychromators. For these experiments, laser pulses occurred at a 30 Hz repetition rate. In addition to performing T_e and n_e calculations for each pulse, the real-time system archived the polychromator signals at the end of each discharge, thereby enabling a post-mortem assessment of the real-time calculations. In this paper, we describe this assessment, with a focus on the methods used for processing the raw polychromator signals. In Sec. II, we assess the peak detection method originally developed for the NSTX-U setup, as well as two additional integration-based methods that are closer to the typical signal processing used at LHD. Then, in Sec. III, we compare the values of T_e derived from each of these methods with the values calculated by the standard LHD methods performed after each discharge.

^{a)}Electronic mail: khammond@pppl.gov

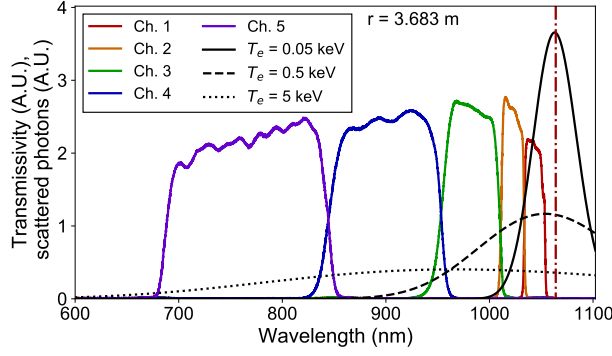


FIG. 2. Transmissivity spectra of the five channels of the polychromator surveying the scattering volume at $r = 3.683$ m, along with Thomson scattering spectra for three example electron temperatures.

II. SIGNAL PROCESSING METHODS

The real-time system computes T_e and n_e values in a least-squares spectral fitting technique that optimizes T_e and a scaling factor c to minimize χ^2 , defined as follows:

$$\chi^2 = \sum_{i=1}^{N_c} \frac{(s_i - cF_i(T_e))^2}{\sigma_{s_i}^2 + s_i^2 \sigma_{F_i}^2} \quad (1)$$

Here, N_c is the number of polychromator channels (five for LHD) and $F_i(T_e)$ is the expected relative signal strength from the i th channel for electron temperature T_e . The electron density n_e can then be determined from c along with calibration data. s_i is a measure of the signal strength from the i th polychromator channel. σ_{s_i} is the standard error in the s_i measurement, and σ_{F_i} is the (dimensionless) fractional error in F_i .

As described in Ref. 7, the values of F_i are pre-computed for a range of T_e by integrating the measured transmissivity spectrum of the i th polychromator channel with the Thomson scattering spectrum as predicted by the Selden model.¹⁶ Fig. 2 shows measured transmissivity curves for the channels of one polychromator, along with scattering spectra for selected values of T_e . Evaluation of $F_i(T_e)$ between laser pulses simply involves querying a look-up table of the pre-computed values. The first derivative of $F_i(T_e)$, also required for the fitting procedure, is estimated via finite differencing.

s_i in Eq. 1 must be proportional to the number of scattered photons received by the channel. In this section, we will describe three procedures that we have implemented for deriving values for s_i from time-resolved polychromator signals and compare their accuracy and computational requirements. The procedures, which include peak detection, direct integration, and curve fitting, are displayed schematically in Fig. 3 for two examples of raw signals from a polychromator channel.

A. Peak detection

As originally designed, the real-time processing code worked on the assumption that the integrated photon flux to each polychromator channel would scale directly with the peak amplitude of the raw signal. Hence, it would be sufficient to define the signal strengths s_i simply as the peak amplitudes in order to determine T_e . Provided that the signals from Rayleigh and/or Raman calibrations are evaluated in the same way, a consistent scaling factor may be determined for extracting n_e from the scaling parameter c .

The real-time code determines the amplitude of the scattered-light signal during each laser pulse by subtracting the peak value of the signal from the average of the background signal recorded prior to the laser pulse. The procedure is illustrated in Fig. 3a for the case of a single laser pulse and in Fig. 3d for a case when two lasers were fired in rapid succession. To correct for stray laser light due to reflections within the plasma vessel, this amplitude would be adjusted by subtracting the average signal amplitude recorded during laser pulses prior to the beginning of the discharge.

This approach has the advantage of simplicity, and, therefore, computational speed. However, the amplification circuitry, which in this setup includes a high-pass filter to reduce the background level, may exhibit a dispersive or nonlinear response that would give rise to distortions of the scattered light signal that can vary from one channel to another.

The effect of such distortions in the fitting of the polychromator output spectra is visible in Fig. 4a, which compares fitted data s_i/c with the predicted signals $F_i(T_e)$ acquired from one scattering volume during an example plasma discharge. These fits contain substantial systematic errors. In particular, the fitted signal amplitudes are mostly lower than the model prediction for polychromator channels 3 and 5, whereas they are mostly higher than the model prediction for polychromator channel 4. Interestingly, there there appears to be no clear difference in the offsets observed for the single- and double-laser-pulse data.

B. Numerical integration

In the presence of distorted signals from the polychromator, the integrals of the signals may provide a more accurate representation of the detected scattered light than the amplitudes alone. To test this, we implemented a modified version of the signal processing function that performs trapezoidal integration on an interval of the signal of pre-determined length centered around the peak value. This procedure is illustrated schematically in Fig. 3b and 3e. Analogously to the case of pulse amplitude determination, the integrals of signals recorded during the plasma discharge were corrected by subtracting the average integral value of a set of stray laser light signals obtained before the beginning of the plasma discharge.

The switch from pulse-amplitude determination to numerical integration has minimal impact on computation time, which is an important consideration for real-time applications. The time for each numerical integration was typically $\leq 1 \mu\text{s}$.

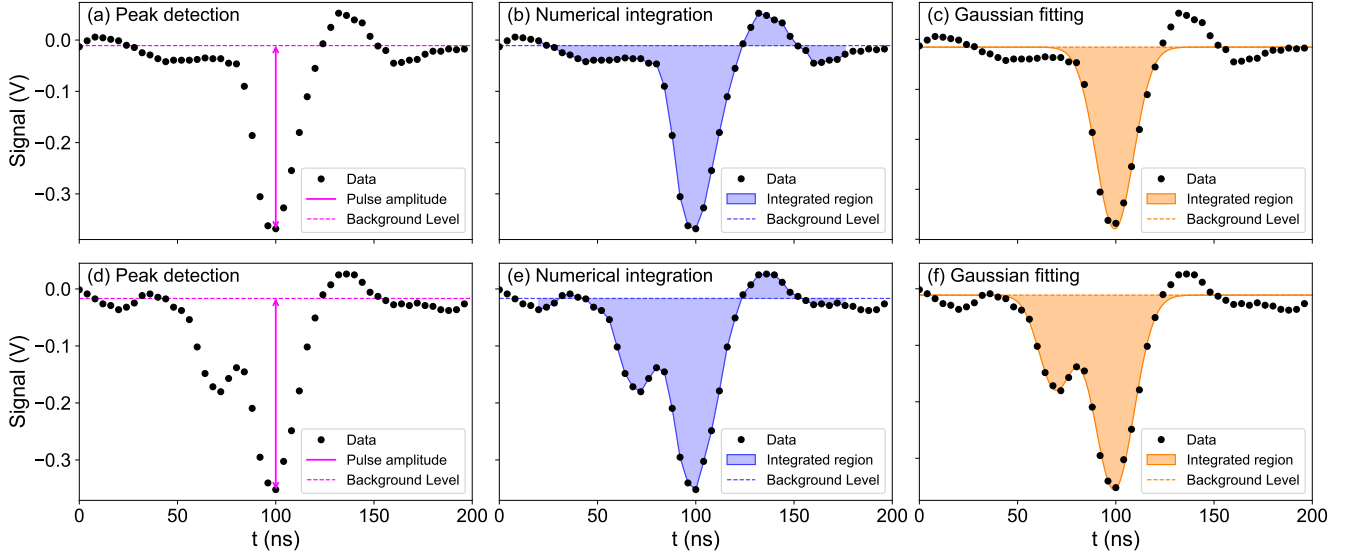


FIG. 3. Typical signal from a polychromator channel along with depictions of the three methods for evaluation considered in this work: (a) peak detection, (b) numerical integration, and (c) Gaussian curve-fitting for a signal arising from light scattered from a single laser pulse; (d)-(f) like (a)-(c) but for a signal arising from light scattered from two overlapping laser pulses.

greater than the time for amplitude determination; hence, to evaluate the five polychromator outputs necessary for a spectral fit, the added time would not exceed $5 \mu\text{s}$. This is negligible compared to the laser firing period of 16.7 ms for which the system was designed.

As shown in Fig. 4b, the use of integrated signals improved the quality of the spectral fits. In particular, the systematic offsets between the data and the fitted spectra that arose from the use of pulse amplitudes (Fig. 4a) are no longer visible.

While the use of numerical integration resolved the issue of systematic offsets between the fitted data and calculated spectra, the fits did exhibit increased scatter, particularly for the relatively weak signals from polychromator channel 5. This may arise from background noise, which can make spurious contributions to the integral in the case of a low signal-to-noise ratio (SNR). This effect can be visualized in Fig. 3b and 3e. As the background fluctuations in the raw signal exhibit time scales similar to the laser pulse width, the contributions from these fluctuations to the integral will not necessarily cancel out. Direct integration will also take a contribution from a brief overshoot of the background level following the signal pulse, an effect of the amplifier circuitry. This may result in systematic underestimates of the integrated photon flux, although the effect is not fully understood.

C. Curve fitting

One way to avoid contributions from background fluctuations is to use the integral of a waveform fitted to the signal rather than the integral of the raw signal itself.^{17,18} To this end, we implemented an additional function that fits Gaussian

curves to the raw signal and outputs the integrals computed analytically from the fitting parameters. Specifically, signals from single laser pulses were fit to functions of the form

$$f_{\text{single}}(t) = p_1 + p_2 \exp \left[-\frac{(t - p_4)^2}{2p_3^2} \right] \quad (2)$$

with free parameters $p_{1..4}$, and signals arising from double laser pulses were fit to functions of the form

$$f_{\text{double}}(t) = p_1 + p_2 \exp \left[-\frac{(t - p_4)^2}{2p_3^2} \right] + p_5 \exp \left[-\frac{(t - p_7)^2}{2p_6^2} \right] \quad (3)$$

with free parameters $p_{1..7}$. The true signal waveform is not expected to exactly match the Gaussian form of the laser pulse due to the effects of the amplifier circuitry. However, a more precise model would be more computationally expensive, and we expect that the Gaussian fits will provide sufficient accuracy for the purposes of real-time analysis.

The parameters p_i are determined in a least-squares fitting procedure. The integrals of the fitted curves follow from the parameters as $\sqrt{2\pi}p_2p_3$ for single pulses and $\sqrt{2\pi}(p_2p_3 + p_5p_6)$ for double pulses. The choice of whether to fit to f_{single} or f_{double} can be made based on signals recording the energy of the lasers, which the system also uses in the calculation of n_e : if two laser energy channels record nonzero signals, f_{double} is employed; otherwise, f_{single} is applied.

The success of the fits relies upon reasonable choices of initial guesses for the free parameters. Initial values for the background level p_1 , amplitude p_2 , and time offset p_4 can be determined easily from the peak-detection and background

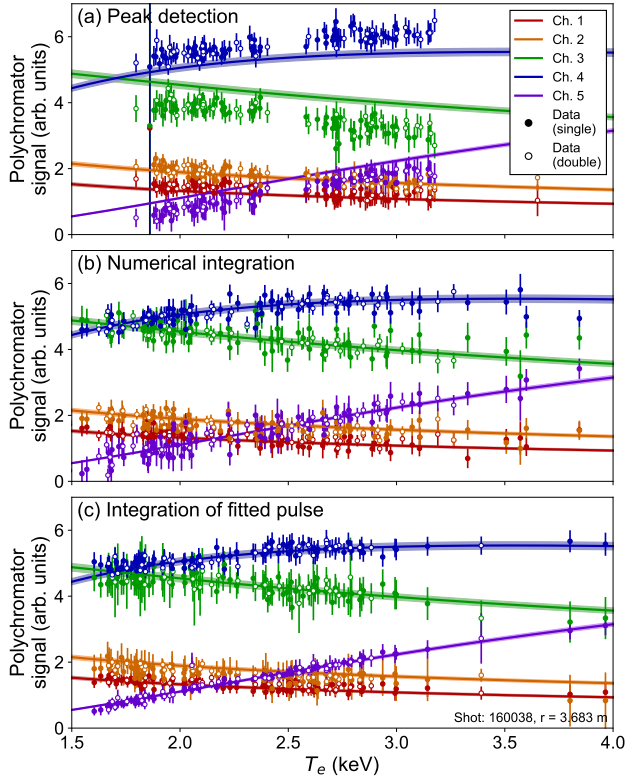


FIG. 4. Comparison of calibration spectra with fitted polychromator signals collected from the scattering volume at $r = 3.683$ m, near the magnetic axis. Solid curves represent the expected relative signals $F_i(T_e)$ from each polychromator channel. Circles represent the signals s_i from each channel, divided by the scaling factor c and positioned to T_e according to their respective spectral fits. Filled circles arise from single laser pulses; open circles arise from double pulses. (a) Signals determined through peak detection; (b) numerical integration; and (c) integration of an integrated Gaussian fit curve.

averaging procedures described in Sec. II A. Since the pulse widths are relatively consistent across laser pulses, the parameter p_3 (and p_6 for double pulses) is initialized to a preset value. Finally, for double pulses, the time offset p_7 is initialized based on a preset fixed offset relative to p_4 and the amplitude p_5 is initialized based on a preset ratio to p_2 .

While this curve-fitting approach usually yields a more accurate estimate of the scattered light received by each polychromator channel than simple integration, the procedure requires more computation time. Within each least-squares iteration, the exponential function must be evaluated at least twice for every time point within the integration window. In addition, an $n \times n$ matrix inversion must be performed, where n is the number of free parameters. With good choices of initial guesses, fits typically require three to five iterations to converge. We employed the Armadillo C++ linear algebra library^{19,20} to ensure efficient matrix inversion.

A survey of processing times over five example shots indicated that 95% of fits of signals to f_{single} took less than $30 \mu\text{s}$. Fits to f_{double} took less than $65 \mu\text{s}$ for 75% of signals and

less than $175 \mu\text{s}$ for 95% of signals. The time to process the signals from five polychromator channels, then, would be $\leq 150 \mu\text{s}$ for single laser pulses and $\leq 875 \mu\text{s}$ for double laser pulses. Given that the system was previously qualified to perform all data acquisition and analysis within 16.7 ms or less (a 60 Hz repetition rate) with the pulse amplitude method, it should still be able to accommodate a 30 Hz repetition rate even with an additional 1 ms for curve fitting.

III. TEMPERATURE MEASUREMENT COMPARISON

Fig. 5 shows a comparison of temperature estimates using scattered light signal levels evaluated with the three different methods described in Sec. II. Fig. 5a shows the temperatures determined for the scattering volume near the magnetic axis at $r = 3.683$ m during discharge 160038. As a reference, we have also included values output from the standard LHD post-processing software. Fig. 5b shows the differences between T_e evaluated by the three methods and the reference post-processed values for each laser pulse.

Overall, the values of T_e as computed by all three methods track well with the reference values, almost always agreeing to within 0.5 keV. However, the sources of error for the pulse amplitude and numerical integration methods as discussed in Sec. II A and II B are also apparent. The values determined from the pulse amplitudes exhibit a positive discrepancy (288 ± 181 eV) with the reference values arising from systematic errors in the spectral fitting. The values determined from numerical integration exhibit a larger scatter (standard deviation of 280 eV) than the other two methods due to the impacts of noise on the integration. Finally, the values of T_e determined through Gaussian curve fitting exhibit a level of scatter (207 eV) closer to the pulse amplitude approach (181 eV) but without a systematic offset from the reference values. The tendency of curve-fitting analysis methods to produce T_e values with less scatter than direct signal integration has also been observed, for example, in the Thomson scattering system at KSTAR.²¹

IV. CONCLUSIONS AND FUTURE WORK

In summary, we have adapted and commissioned a real-time evaluation system for Thomson scattering on the LHD experiment, representing the first *in situ* operation of the system. We have implemented and compared three different approaches to evaluating the polychromator signals, each of which offers advantages and disadvantages. The curve fitting approach generally provides the greatest accuracy and precision, but at the expense of extra computational time. For all methods, isolated spikes in the fitted temperature due to unexpected features in the signal are rare but unlikely to be completely avoidable. Hence, filtering of the output—through circuitry or additional software features—is advisable. Nevertheless, initial comparisons of T_e output by all three methods mostly exhibit good agreement with values calculated by the standard post-processing software.

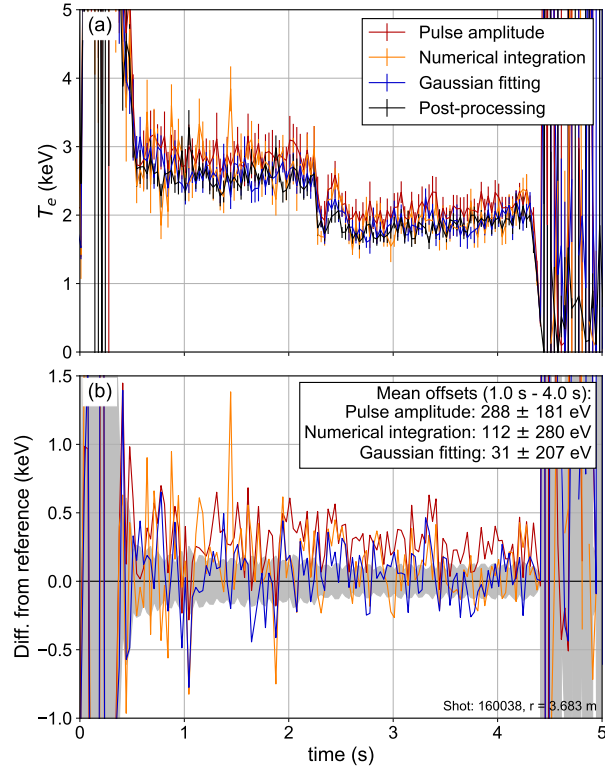


FIG. 5. Comparison of T_e calculated by the standard LHD post-processing routines to T_e calculated by functions from the real-time code employing different methods for handling polychromator signals. (a) T_e calculated for the scattering volume at $r = 3.683$ m during discharge number 160038; (b) Difference between T_e calculated by the different methods and the post-processing values. The shaded region indicates the uncertainty of the post-processing values. The means and standard deviations of the differences for the methods for samples between 1.0 s and 4.0 s are shown in the inset.

In addition to providing estimating T_e , the system calculates n_e for each laser pulse using the fitting parameter c (Eq. 1) along with data from Rayleigh or Raman calibrations. Next steps will include benchmarking n_e output against the values from standard Thomson post-processing. We then plan to utilize the system's outputs to assist in experiments. One application will be to provide input for regulation of the electron temperature profile with electron cyclotron heating. The system may also help to inform experiments to shape the density profile with pellet fueling. The findings in this study will also inform the deployment of the original implementation of the system in the upcoming operation phase of NSTX-U.

ACKNOWLEDGMENTS

The authors would like to thank B. P. LeBlanc for the helpful discussions. This work was supported by the US Department of Energy under contracts DE-AC02-09CH11466 and DE-SC0015480. The data that support the findings of this study are available from the corresponding author upon reasonable request.

- ¹I. Hutchinson, *Principles of Plasma Diagnostics*, 2nd ed. (Cambridge University Press, 2002).
- ²C. M. Greenfield, G. L. Campbell, T. N. Carlstrom, J. C. DeBoo, C.-L. Hsieh, R. T. Snider, and P. K. Trost, *Review of Scientific Instruments* **61**, 3286 (1990).
- ³S. Shibaev, G. Naylor, R. Scannell, G. McArdle, T. O'Gorman, and M. J. Walsh, *Fusion Engineering and Design* **85**, 683 (2010).
- ⁴S. Shibaev, G. Naylor, R. Scannell, G. J. McArdle, and M. J. Walsh, in *Proceedings of the 17th IEEE-NPSS Real Time Conference* (2010).
- ⁵E. Kolemen, S. L. Allen, B. D. Bray, M. E. Fenstermacher, D. A. Humphreys, A. W. Hyatt, C. J. Lasnier, A. W. Leonard, M. A. Makowski, A. G. McLean, R. Maingi, R. Nazikian, T. W. Petrie, V. A. Soukhanovskii, and E. A. Unterberg, *Journal of Nuclear Materials* **463**, 1186 (2015).
- ⁶H. Arnichand, Y. Andrebe, P. Blanchard, S. Antonioni, S. Couturier, J. Decker, B. P. Duval, F. Felici, C. Galperti, P.-F. Isoz, P. Lavanchy, X. Llobet, B. Marlétaz, P. Marmillod, J. Masur, and the TCV team, *Journal of Instrumentation* **14**, C09013 (2019).
- ⁷F. M. Laggner, A. Diallo, B. P. LeBlanc, R. Rozenblat, G. Tchilinguirian, E. Kolemen, and the NSTX-U team, *Review of Scientific Instruments* **90**, 043501 (2019).
- ⁸R. Rozenblat, E. Kolemen, F. M. Laggner, C. Freeman, G. Tchilinguirian, P. Sichta, and G. Zimmer, *Fusion Science and Technology* **75**, 835 (2019).
- ⁹I. Yamada, H. Funaba, R. Yasuhara, H. Hayashi, N. Kenmochi, T. Minami, M. Yoshikawa, K. Ohta, J. H. Lee, and S. H. Lee, *Review of Scientific Instruments* **87**, 11E531 (2016).
- ¹⁰K. Narihara, K. Yamauchi, I. Yamada, T. Minami, K. Adachi, A. Ejiri, Y. Hamada, K. Ida, H. Iguchi, K. Kawahata, T. Ozaki, and K. Toi, *Fusion Engineering and Design* **34-35**, 67 (1997).
- ¹¹K. Narihara, I. Yamada, H. Hayashi, and K. Yamauchi, *Review of Scientific Instruments* **72**, 1122 (2001).
- ¹²I. Yamada, K. Narahara, H. Funaba, T. Minami, H. Hayashi, T. Kohmoto, and the LHD experiment group, *Fusion Science and Technology* **58**, 345 (2010).
- ¹³I. Yamada, K. Narihara, H. Hayashi, H. Funaba, and the LHD experiment group, *Plasma and Fusion Research* **2**, S1106 (2007).
- ¹⁴B. P. LeBlanc, R. E. Bell, D. W. Johnson, D. E. Hoffman, D. C. Long, and R. W. Palladino, *Review of Scientific Instruments* **74**, 1659 (2003).
- ¹⁵A. Diallo, B. P. LeBlanc, G. Labik, and D. Stevens, *Review of Scientific Instruments* **83**, 10D532 (2012).
- ¹⁶A. C. Selden, *Physics Letters* **79A**, 405 (1980).
- ¹⁷B. Kurzan, M. Jakobi, H. Murmann, and the ASDEX Upgrade team, *Plasma Physics and Controlled Fusion* **46**, 299 (2004).
- ¹⁸S. A. Bozhnikov, M. Beurskens, A. Dal Molin, G. Fuchert, E. Pasch, M. R. Stoneking, M. Hirsch, U. Höfel, J. Knauer, J. Svensson, H. Trimiño Mora, R. C. Wolf, and the W7-X team, *Journal of Instrumentation* **12**, P10004 (2017).
- ¹⁹C. Sanderson and R. Curtin, *Journal of Open Source Software* **1**, 26 (2016).
- ²⁰C. Sanderson and R. Curtin, "A user-friendly hybrid sparse matrix class in C++," (Springer, 2018) p. 422.
- ²¹J. H. Lee, H. J. Kim, I. Yamada, H. Funaba, Y. G. Kim, and D. Y. Kim, *Journal of Instrumentation* **12**, C12035 (2017).